

Adaptive Modular Multilevel Converter Model for Electromagnetic Transient Simulations

Anton Stepanov, *Student Member, IEEE*, Jean Mahseredjian, *Fellow, IEEE*, Ulas Karaagac, *Member, IEEE*, Hani Saad, *Member, IEEE*

Abstract—This paper proposes an adaptive model of modular multilevel converter (MMC) for electromagnetic transient (EMT) simulations. The model is applicable to MMCs with arbitrary numbers of half-bridge and full-bridge submodules. The proposed design includes average value model, arm equivalent model, and detailed equivalent model. It allows smoothly transitioning from one model to another during time-domain simulations depending on the desired accuracy and execution time constraints.

Modifications required in conventional MMC models to achieve smooth transitions are presented in the paper. Time-domain initialization methods are developed for each constituting model, including initialization of the appropriate control system blocks. Validity and effectiveness of the proposed adaptive model is demonstrated using EMT simulations of 401-level MMC-HVDC system.

Index Terms—adaptive model, average value model, arm equivalent, detailed equivalent, High-Voltage Direct Current, model switching, modular multilevel converter, simulation

I. INTRODUCTION

Modular multilevel converters (MMCs) have become the state-of-the-art technology for HVDC systems. A typical MMC in HVDC applications has six arms of series-connected submodules (SMs), each providing one step in the resulting multilevel AC waveform, Fig. 1. Due to its advantages over conventional two- and three-level converters, including easier scalability to higher voltages, lower harmonic content, better reliability, lower switching frequency and voltage [1], [2], MMCs are used in modern HVDC projects [3], [4].

Different MMC models for electromagnetic transient (EMT) simulations are available in the literature and the choice of the model represents a compromise between the necessary accuracy and computational burden:

- The detailed model (DM) includes nonlinear IGBT v-i characteristics and offers the highest degree of precision in EMT studies [5]. It can be used for validation of simplified models, for SM-level studies, and for internal fault studies [6].

A. Stepanov and J. Mahseredjian are with the Department of Electrical Engineering, Polytechnique Montréal, Montreal, QC H3T 1J4, Canada (e-mail: anton.stepanov@polymtl.ca; jeanm@polymtl.ca).

U. Karaagac is with the Department of Electrical Engineering, Hong Kong Polytechnic University, Hung Hom, Kowloon, Hong Kong (e-mail: ulas.karaagac@polyu.edu.hk).

H. Saad is with the Réseau de Transport d'Electricité, Paris 92932, France (e-mail: hani.saad@rte-france.com).

- The detailed equivalent model (DEM) simplifies IGBT switch representation to two-value resistances [5], [7]. All SM voltages and gating signals are available. It is often implemented independently and is interfaced with the main EMT solver using a two-port Thevenin or Norton equivalent circuit so internal electrical nodes are inaccessible [6].
- The arm equivalent model (AEM) assumes that all SMs in each arm are perfectly balanced, so only one equivalent capacitor is used to represent the whole arm [8]. Grid studies and controller design can be performed with such a model [6].
- The average value model (AVM) is composed of two parts, AC and DC, disconnected from each other and aggregates SM capacitors of all arms into a single DC side capacitor. Neither voltage ripple nor circulating current are available but AC and DC currents and voltages in normal balanced operating conditions are sufficiently accurate [5], [9].

EMT simulation studies of power systems can provide accurate results over a wide frequency range, especially if small time-steps are used, but high accuracy increases computing times. Many methods have been proposed in the literature to accelerate time-domain simulations of MMCs, including various improvements to standalone models [8, 10-13].

The method presented in this paper provides acceleration based on the assumption that during time-domain simulations there could be intervals during which the details of converter internal behavior can be ignored. Initialization and slower electromechanical transients constitute such intervals. It is then possible and sufficient to model accurately only converter's external behavior to accelerate computations, which makes the proposed new relaxation method an additional improvement to existing acceleration methods.

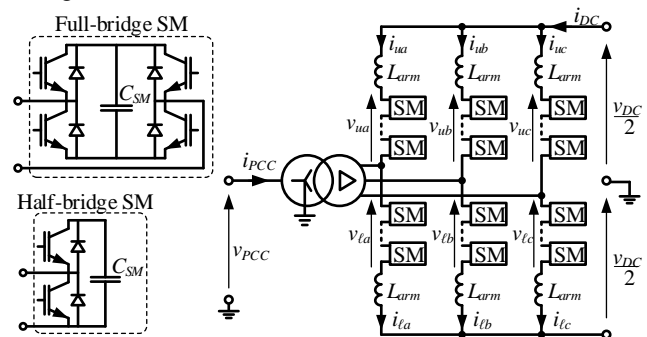


Fig. 1. Typical three-phase MMC topology with a coupling transformer.

Not much research is available in the literature on this topic. In [14] and [15] it is proposed to switch between the DEM and

AEM, but the AVM and its controls are not considered. Neither [14] nor [15] pays much attention to the capacitor balancing block effects on the SM voltages **during DEM activation: all voltages are considered identical in each arm of the DEM when it is activated**, which is not realistic. Besides, [14] only focuses on half-bridge (HB) SMs and [15] **states** that in normal operation **of the AEM** all types of SMs behave like HB SMs and the possibility of negative insertion of full-bridge (FB) SMs **has not been demonstrated for the AEM in normal operation. Moreover, the effects of capacitor balancing among HB and FB parts have not been considered for the AEM in [15].** None of the papers discuss automated switching **between models**.

This paper presents an adaptive MMC model that allows switching between the AVM, AEM, and DEM versions. It is applicable for HB, FB, and hybrid configurations with arbitrary proportions of HB and FB SMs. Two novel AVMs as well as an automated AVM activation scheme are proposed. Switching between different control systems is also considered. Validation of the proposed adaptive model and evaluation of computational time gains are based on the simulation of realistic test cases. The adaptive model can also be **applicable** in real-time simulations when the available computational power is limited and only few converters can be modeled in detail.

This paper starts in section II with the overview of the proposed model and implementation details. Section III presents methods for switching between the detailed and simplified parts of the adaptive model. Section IV shows EMT simulations of 401-level MMC HVDC systems.

II. ADAPTIVE MMC MODEL

The schematic diagram of the proposed adaptive model is shown in Fig. 2. Activation of any model requires initialization of the appropriate control system blocks and deactivation of other MMC models. The control system in Fig. 2a is based on the generic cascade control system of [9] and includes circulating current suppression control (CCSC), capacitor balancing algorithm (CBA), and nearest level control (NLC).

To simplify the process of switching between models, all models must have identical electrical interface (i.e. connected to the same nodes). In the DEM and AEM, each arm is interfaced with the network using a two-port equivalent circuit whereas conventional DM and AVM have a significantly different structure. The DM has all its internal nodes available to the solver and the AVM has separate AC and DC circuits [5].

Since DM applications in grid studies are limited [6], it is not included in the proposed adaptive MMC model. The AVM is adapted to match the DEM and AEM interfaces (Section II.B).

One arm of the adaptive MMC model is shown in Fig. 2b. All three model blocks are connected in parallel but only one is active at any given time. The active model recalculates its Norton equivalent at each time-point **and** the two inactive models supply zero equivalent admittance and current between their nodes. Each white block in Fig. 2 is implemented in a DLL (Dynamic-Link Library) to facilitate activation/deactivation.

In the following, lowercase letters represent variables, capital letters represent constants, and bold capital letters represent arrays of variables.

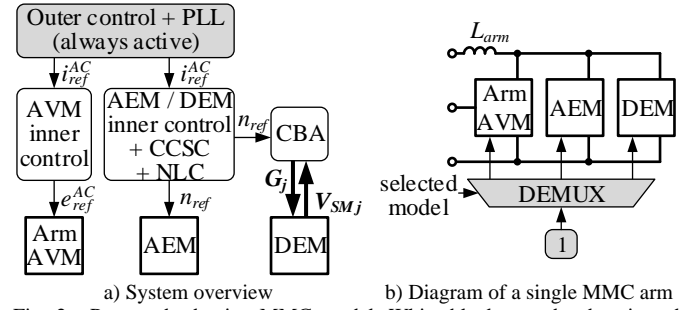


Fig. 2. Proposed adaptive MMC model. White blocks can be deactivated. Demultiplexer DEMUX allows to send the activation signal “1” to the required model based on the selected model type.

A. Control System

The standard cascade control system is considered [9]. The part of the control system that is common to all models is always kept active. It includes a PLL (Phase-Locked Loop) for grid synchronization and an outer control loop that can control active and reactive powers, and DC and AC voltage magnitudes. The outer loop generates the AC side current references i_{ref}^{AC} for the inner control loop (Fig. 2a). Other blocks in the control system are activated and deactivated at runtime depending on the selected model.

The inner control loop for the AVM produces AC side EMF references e_{ref}^{AC} that are supplied to the model. Also, in this paper it is supposed that the AVM is used in balanced grid conditions, so only positive sequence control is considered.

The AEM and DEM can be used during grid unbalance, so inner control also considers negative sequence. With AEM and DEM, the output of the inner control loop is arm switching function reference s_{ref} . Therefore, two different inner control blocks are shown in Fig. 2a. Additionally, the AEM and DEM require CCSC and NLC that calculates the number n_{ref} of SMs to insert at each time-point [9].

The DEM requires individual SM-level control and CBA for generating gating signals G_j for IGBTs based on n_{ref} and capacitor voltages V_{SMj} (j is SM index).

As it has been mentioned, this paper deals only with the standard cascade control system. If other controls are used in a simulation, such as the energy control for the AEM and DEM, their internal variables should also be initialized when the corresponding constituting model is activated to minimize the transient following the activation.

B. AVM

The conventional AVM consists of two electrical circuits disconnected from each other: three-phase AC and single-phase DC equivalent circuits [9]. In more detailed models, current flowing through the arm inductance L_{arm} is the sum of AC and DC currents. To avoid arm current discontinuity and to reduce topological differences between models, two arm AVMs are proposed in this section.

Two models are proposed because two options are considered regarding placement of the arm inductor L_{arm} : the reactor can be connected either to the DC bus, as in [16], [17],

in which case the chain of SMs is connected to the AC bus. Otherwise, L_{arm} can be connected to the AC bus, as in [18], [19] and SM chain is connected to the DC bus. Conventional MMC models are readily applicable in both cases. However, the topology of the proposed arm AVMs changes depending on the position of the arm inductor because it dictates if the arm AVMs are connected to each other via the AC or the DC side.

It should be noted that although the arm AVMs are modeling each arm of the MMC separately, they still have to be connected to each other as shown in Fig. 3 and Fig. 4, and therefore should only be used to represent the whole converter, contrary to the DEM or AEM, where any arm can be modeled independently from others. The arm AVMs can be used in the same context as the conventional AVM.

The blocked mode is not included in the proposed arm AVMs because the AVM is known to be inaccurate in this operation mode [5]. Therefore, if the blocked mode has to be activated, it is proposed to switch to a more detailed model, such as the AEM.

1) Arm-AVM-1

The Arm-AVM-1 can be used if L_{arm} is connected to the DC bus, as in Fig. 1. Each arm of the Arm-AVM-1 consists of two branches: the main AC branch and the auxiliary DC branch.

The auxiliary branch represents the DC side of the conventional AVM [5]. The value of the arm AVM capacitor C_{AVM} can be found using energy conservation principle [9]:

$$C_{AVM} = 4 C_{SM} / N_{SM} \quad (1)$$

where C_{SM} is SM capacitance, N_{SM} is SM count per arm.

The current reference i_{ref}^{DC} in the auxiliary branch is identical for all six arms and is obtained using the power balance principle, i.e. power generated at the AC side must match the power consumed at the DC side. It is assumed for simplicity that instantaneous AC side EMF e^{AC} is equal to its reference value e_{ref}^{AC} . The current reference is then obtained from

$$i_{ref}^{DC} = \sum_k (e_{ref_k}^{AC} i_{arm_k}^{AC}) / \sum_k v_{C_{AVM_k}} \quad (2)$$

where i_{arm}^{AC} is the current in the main branch, $v_{C_{AVM}}$ is the voltage of C_{AVM} capacitor, and $k = 1 \dots 6$ is the arm index.

The resistance R_{arm} represents conduction losses and can be calculated from

$$R_{arm} = R_{ON} (N_{HB} + 2N_{FB}) \quad (3)$$

where R_{ON} is the ON-state resistance of IGBT switches, N_{HB} and N_{FB} are the numbers of HB and FB SMs per arm.

The main branch is composed of the arm resistance R_{arm} and two controlled voltage sources: the DC voltage source reference e_{ref}^{DC} is measured in the auxiliary branch and used to divert the DC component of arm current to the auxiliary branch (it should be noted that there is a single time-step delay between measurement and controlled voltage source command). The AC voltage reference e_{ref}^{AC} is provided by the control system (see Fig. 2a) and is used to fulfill desired control objectives at

converter terminals (see section II.A). The AC voltage references e_{ref}^{AC} in the upper and lower arms of each phase have 180° phase-shift whereas the DC voltage references e_{ref}^{DC} are identical and are equal to $v_{DC} / 2$ in steady-state. The Arm-AVM-1 is shown in Fig. 3.

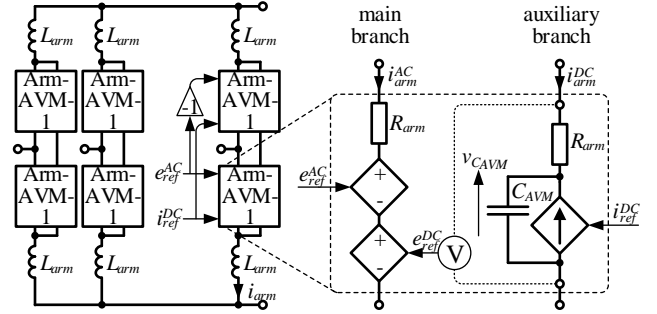


Fig. 3. Schematic electrical diagram of Arm-AVM-1.

2) Arm-AVM-2

The Arm-AVM-2 is applicable in the case when the arm inductor L_{arm} is connected to the AC terminals of the MMC. Equations (1)–(3) are still valid, but the model consists of fewer elements and the connections are different, as shown Fig. 4.

Also, contrary to the Arm-AVM-1 described in the subsection II.B.1, current references i_{ref}^{DC} for lower and upper arms are now different: reference signal for lower arms is provided by (2), whereas the reference signal for the upper arms has a negative sign $-i_{ref}^{DC}$. Upper and lower arms of each phase use the same AC voltage reference e_{ref}^{AC} .

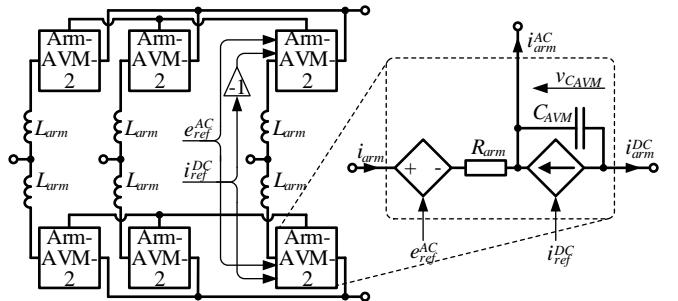


Fig. 4. Schematic electrical diagram of Arm-AVM-2.

C. Hybrid-AEM

The AEM combines all SMs in each arm into an equivalent circuit [5]. In this article, the Hybrid-AEM comprises both HB and FB SMs. HB and FB parts must be treated separately because their behavior differs in blocked mode and when SMs are to be inserted negatively (so only FB SMs can be inserted).

1) Equivalent Electrical Circuit

The proposed Hybrid-AEM can operate in two states: active and high impedance. In active operation, Thevenin equivalents are found using trapezoidal integration rule [20]. For HB part:

$$r_{th HB} = R_{ON} N_{HB} + n_{HB}^2 R_C / N_{HB} \quad (4)$$

$$v_{th HB} = n_{HB} \hat{v}_{HB} \quad (5)$$

For FB part:

$$r_{th FB} = 2R_{ON} N_{FB} + n_{FB}^2 R_C / N_{FB} \quad (6)$$

$$v_{th FB} = n_{FB} \hat{v}_{FB} \quad (7)$$

where $r_{th\ HB}$ and $r_{th\ FB}$ are Thevenin equivalent resistances; $v_{th\ HB}$ and $v_{th\ FB}$ are Thevenin equivalent voltages for HB and FB parts, respectively; $R_C = 0.5\Delta t / C_{SM}$ is SM capacitor discretization resistance and Δt is the time-step; n_{HB} and n_{FB} are the numbers of HB and FB SMs to insert; \hat{v}_{HB} and \hat{v}_{FB} are HB and FB history voltages which are calculated at each time-point as:

$$\hat{v}_{HB} = v_{HB} + n_{HB} i_{arm} R_C / N_{HB} \quad (8)$$

$$\hat{v}_{FB} = v_{FB} + n_{FB} i_{arm} R_C / N_{FB} \quad (9)$$

where v_{HB} and v_{FB} are HB and FB voltages.

If the Hybrid-AEM is in high impedance state (blocked mode), the Thevenin equivalent circuits are calculated as

$$r_{th\ HB} = R_{OFF} N_{HB} \quad (10)$$

$$r_{th\ FB} = 2R_{OFF} N_{FB} \quad (11)$$

$$v_{th\ HB} = v_{th\ FB} = 0 \quad (12)$$

where R_{OFF} is the IGBT OFF-state resistance.

The final Norton equivalent of the Hybrid-AEM that is supplied to the EMT solver is obtained from the series connection of the HB and FB Thevenin equivalents (4)–(7).

2) Blocked Mode

In the blocked mode, SM insertion is determined by the arm current direction and capacitor voltage of each equivalent part (HB or FB). The proposed algorithm is as follows:

1. Get arm voltage v_{arm} from the EMT solver.
2. Assign switch states according to i_{arm} direction at the previous time-point and recalculate i_{arm} . If calculated i_{arm} direction matches switch states, set n_{HB} and n_{FB} . Exit.
3. If not, assign switch states using opposite current direction and recalculate i_{arm} . If new current direction matches switch states, set n_{HB} and n_{FB} according to the switch states. Exit.
4. If it is impossible to match i_{arm} direction and switch states, assign high-impedance state, $n_{HB} = n_{FB} = 0$.

To find an accurate solution in blocked mode, the AEM requests the EMT core to iterate if the arm current direction or the type of blocked mode changes from the previous time-point. Since there is no guarantee that such process converges, the limit number of iterations is set to 30. In all performed tests the number of iterations never reached above 6.

Each arm performs this algorithm independently from others. The value of i_{arm} at steps 2 and 3 is calculated considering (4)–(7) either with $n_{HB} = N_{HB}$ and $n_{FB} = N_{FB}$ (for the positive direction) or $n_{HB} = 0$ and $n_{FB} = -N_{FB}$ (for the negative one). For the positive direction:

$$i_{arm} = \frac{v_{arm} - [N_{HB} \hat{v}_{HB} + N_{FB} \hat{v}_{FB}]}{R_{ON} [N_{HB} + 2N_{FB}] + R_C N_{SM}} \quad (13)$$

For the negative direction:

$$i_{arm} = \frac{v_{arm} + N_{FB} \hat{v}_{FB}}{R_{ON} [N_{HB} + 2N_{FB}] + R_C N_{FB}} \quad (14)$$

To get the arm current direction it is sufficient to calculate only the numerator in (13) and (14). Fig. 5 shows the steps of the blocked mode algorithm applied to an arm with one HB SM, one FB SM, and positive arm current direction at the previous time-point:

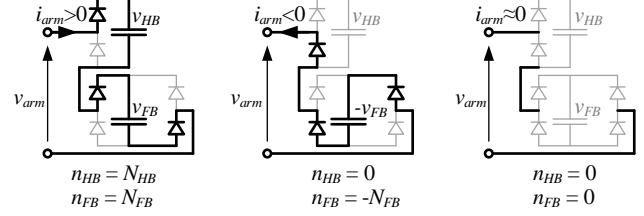


Fig. 5. Blocked mode algorithm for Hybrid-AEM. Left to right: with i_{arm} direction as at the previous time-point; with opposite current direction; high-impedance state. Black lines represent currently active elements.

3) Pseudo-CBA

A Pseudo-CBA is proposed for the Hybrid-AEM in normal operation mode to imitate realistic behavior of hybrid MMCs: Pseudo-CBA defines n_{HB} and n_{FB} at each time-point, Fig. 6.

If n_{ref} is negative, only FB SMs are inserted:

$$n_{HB} = 0 \quad (15)$$

$$n_{FB} = n_{ref} \quad (16)$$

Otherwise, selection depends on v_{HB} , v_{FB} , n_{ref} , and i_{arm} . With positive i_{arm} and $v_{HB} > v_{FB}$, as well as with negative i_{arm} and $v_{HB} \leq v_{FB}$:

$$n_{HB} = \max(0, n_{ref} - N_{FB}) \quad (17)$$

$$n_{FB} = \min(n_{ref}, N_{FB}) \quad (18)$$

In other cases:

$$n_{HB} = \min(n_{ref}, N_{HB}) \quad (19)$$

$$n_{FB} = \max(0, n_{ref} - N_{HB}) \quad (20)$$

To make Pseudo-CBA behavior more realistic, a single time-step delay is applied to the outputs to emulate the time required for the real CBA block to generate gating signals.

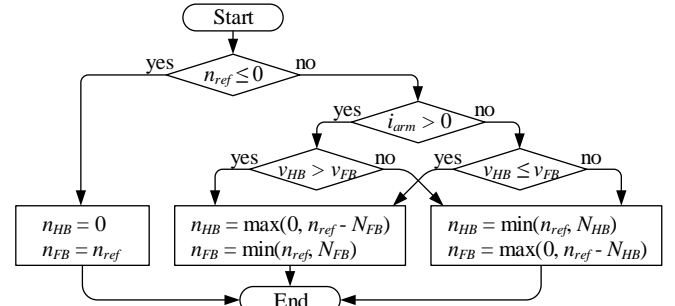


Fig. 6. Proposed Pseudo-CBA algorithm for Hybrid-AEM.

D. DEM

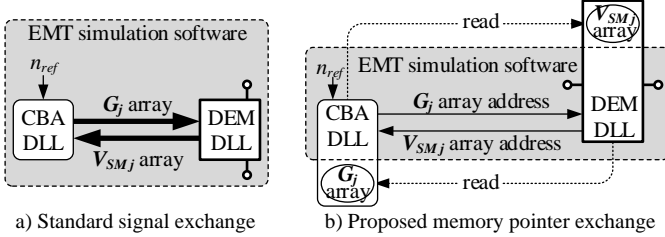
In the DEM, semiconductor switches are represented by two-state resistances: when the switch is conducting, its resistance is low; when the switch is in the OFF-state, its resistance is high (see Table I for numerical values) [5], [7], [10]. Individual SMs voltages and gating signals are available.

Each SM in the DEM requires at least one input (IGBT gating signal) and provides at least one output (capacitor

voltage). The total number of control signals is therefore significant and can be in the order of thousands for each MMC station, which results in long simulation times [16]. Thousands of control signals exchanged between CBA and DEM in the EMT simulation software significantly increase the size of the control system equations matrix which is solved using a generic control system solver (Fig. 7a).

To reduce the number of control signals managed by the EMT software, it is proposed to implement CBA and DEM as DLLs so that they read control signals directly from the memory without soliciting the generic solver, which results in faster simulations. The DLLs exchange the addresses (pointers) of G_j and V_{SMj} arrays through the EMT software (see Fig. 7b). This is labeled as memory pointer exchange.

Other than being useful for acceleration, memory pointer exchange also allows easily changing CBA DLLs at any time during simulation, it is only needed to change the address of the CBA DLL shared memory supplied to the DEM DLL (see example in Fig. 11).



a) Standard signal exchange b) Proposed memory pointer exchange
Fig. 7. Signal exchange between DEM and CBA DLLs. Bold arrows represent multiple signals.

III. INITIALIZATION OF MMC MODELS

The methods for time-domain initialization of constituting models are developed in this section. They allow transitioning from one MMC model to another in any order: AVM to AEM or DEM; AEM to AVM or DEM; DEM to AVM or AEM.

While it is the user who has the ultimate control over the simulation and who decides when to use one or the other constituting model depending on the objectives of the study, some generic guidelines are discussed and an automated activation method for the AVM is proposed in this section.

A. Activation of Arm AVMs

Both arm AVMs proposed in this paper are based on similar electrical circuits and therefore are activated in a similar manner. The only internal variable that needs initialization is the capacitor voltage $v_{C_{AVM}}$. It is supposed that the MMC is at quasi steady-state operation and arm currents and voltages are balanced. In such conditions, there is no current passing through the capacitor C_{AVM} , therefore its voltage can be found using DC current i_{DC} and voltage v_{DC} values:

$$i_{arm}^{DC} = i_{DC} / 3 \quad (21)$$

$$v_{C_{AVM}} = v_{DC} / 2 - R_{arm} i_{arm}^{DC} \quad (22)$$

Before deactivation, the arm AVMs execute the algorithm presented in the appendix that provides the values of capacitor voltages and arm switching functions to more detailed models.

B. Activation of Hybrid-AEM

To activate the Hybrid-AEM, history voltages (8) and (9) are required. They can be found using the values of HB and FB SM voltages, arm current, and the number of SMs to insert. All these variables are already available in the DEM where the number of SMs to insert is provided by the inner control, the arm current is measured directly, and the HB and FB branch voltages can be obtained by averaging individual SM voltages (it is assumed that HB SM voltages are at the beginning of the voltage array, i.e. from $j=1$ to $j=N_{HB}$):

$$v_{HB} = \sum_{j=1}^{N_{HB}} (v_{SMj}) / N_{HB} \quad (23)$$

$$v_{FB} = \sum_{j=N_{HB}+1}^{N_{SM}} (v_{SMj}) / N_{FB} \quad (24)$$

However, if AVM \rightarrow AEM switching is considered, neither capacitor voltages nor the number of SMs to insert is available in advance. Therefore, it is proposed that arm AVMs provide these values using the algorithm from [21], as explained in the appendix. HB and FB voltages are then obtained as

$$v_{HB} = v_{FB} = v_{Ctot} / N_{SM} \quad (25)$$

where v_{Ctot} is sum of all SM voltages per arm.

The number of SMs to insert is found as

$$n_{ref} = \text{round}(s N_{SM}) \quad (26)$$

C. Activation of DEM

Individual history voltages for each SM are necessary to activate the DEM. However, AEM and AVMs can only provide information on the average value of capacitor voltages (in the case of AVMs, the algorithm presented in the appendix is used).

If all SM voltages are set to the same average value, activation procedure is identical to that of the Hybrid-AEM in section III.B and requires the values of capacitor voltage, arm current and inserted SM indices. In this case, a short transient after switching to the DEM can appear [21]. If SM voltages are correctly estimated, such transient can be minimized. Rigorously estimating individual SM voltages can become difficult because their values depend on the type of CBA and may require the knowledge of additional variables.

If a permutation-based CBA is considered, where at each time-point the SM having the highest voltage is swapped with the SM having the lowest voltage when the arm current is positive (the opposite applies when the arm current is negative), the SM voltages are uniformly distributed around the average value [21]. Therefore, it is proposed in this paper to simplify the formula derived in [21] by neglecting the effects of SM insertion on voltage balancing:

$$v_{SMj} = \frac{v_{Ctot}}{N_{SM}} + \left[\frac{j-1}{N_{SM}-1} - \frac{1}{2} \right] i_{arm} s \frac{\Delta t N_{SM}}{N_0 C_{SM}} [1-s] \quad (27)$$

where N_0 is the number of permutations per time-step.

With the voltage sorting-based CBA, the SM voltages are usually considerably closer to each other, so the deviations from the average SM voltage can be neglected

$$v_{SMj} = v_{Ctot} / N_{SM} \quad (28)$$

D. Activation of AVM Inner Control

Inner control can be implemented as a Proportional-Resonant (PR) regulator in α - β frame or as a Proportional-Integral (PI) regulator in d-q frame [22]. In this paper, AVMs are supposed to operate in balanced conditions, so conventional PI control in positive d-q frame is considered.

Contrary to [21], where initialization of PI inner control has been discussed for AEM and DEM, inner control for AVMs produces AC EMF references and not arm switching functions. So, integral history terms for d (H_d) and q (H_q) axes are

$$H_d = v_{PCCd} - e_d + \left[L_{trfo} + L_{arm} / 2 \right] \omega i_q \quad (29)$$

$$H_q = v_{PCCq} - e_q - \left[L_{trfo} + L_{arm} / 2 \right] \omega i_d \quad (30)$$

where L_{trfo} is the transformer inductance; e_d , e_q , i_d , i_q are the AC side EMFs and currents in d-q reference frame; ω is the grid frequency in rad/s.

Projections on d and q axes are obtained by applying Park transformation to three-phase signals: AC side currents are directly available, and AC side EMFs can be obtained as

$$e_m^{AC} = \left[v_{m\ell} - v_{mu} \right] / 2 - R_{arm} i_m / 2 \quad (31)$$

where $m = a, b, c$ is phase index.

E. Activation of AEM / DEM Inner Control

In this paper, inner control based on PR regulators is considered because it can handle positive and negative sequence currents in the same time [22]. Double integral circuit implementation proposed in [21] is taken.

AEM / DEM inner control is activated after AVM has been active. Since AVM is used in balanced grid conditions, only the positive sequence of the first harmonic arm switching functions are considered for initialization. Integral history terms for alpha $H1_\alpha, H2_\alpha$ and beta $H1_\beta, H2_\beta$ channels (as shown in [21]) are

$$H1_\alpha = v_{PCC\alpha} - s_{1\alpha} \quad (32)$$

$$H2_\alpha = \omega \left[v_{PCC\beta} - s_{1\beta} \right] \quad (33)$$

$$H1_\beta = v_{PCC\beta} - s_{1\beta} \quad (34)$$

$$H2_\beta = -\omega \left[v_{PCC\alpha} - s_{1\alpha} \right] \quad (35)$$

where $v_{PCC\alpha}$ and $v_{PCC\beta}$ are PCC voltages in α - β frame, $s_{1\alpha}$ and $s_{1\beta}$ arm switching function first harmonics in α - β frame.

The harmonics of s are found with the algorithm presented in the appendix. Variables $v_{PCC\alpha}$, $v_{PCC\beta}$, $s_{1\alpha}$, and $s_{1\beta}$ are obtained from three-phase signals using Clarke transformation.

For CCSC, second harmonic negative sequence terms of s must be taken, the activation procedure is similar to (29)–(32).

F. Activation of CBA

Voltage sorting CBA and permutation-based CBA [21] are considered in this paper. They do not have history terms, therefore only the initial selection of SMs must be calculated during activation. Considering unequal SM voltage described in the section III.C, uniform SM insertion indices are applied.

G. Selection of the Constituting Models

A fully automatic MMC model selection algorithm would require expert knowledge on system behavior in various conditions, which is often case-specific and is not always available before performing EMT simulations. Besides, the implementation of such an expert knowledge in a control block is expected to result in a relatively complex structure that would still not be able to cover some particular cases.

Therefore, instead of a fully automatic model selection algorithm, an automated AVM activation method is proposed, along with the generic guidelines that would help the user of the proposed adaptive model to decide when to activate one or the other part (AVM, AEM, or DEM).

1) Model Selection Guidelines

The AVM part, which provides the highest acceleration, can be used to rapidly pass through the initialization transient, during the periods when the internal behavior of the converter is not required, and when relatively slow transients, for example electromechanical, are simulated.

The AEM part is suggested to be used in the aforementioned contexts if converter blocking or unbalanced AC grid conditions are expected, which would provide more accurate results on the expense of slightly increasing the computing time. Otherwise, the AEM is suggested to be used when the behavior of lower-level controls, such as CCSC, is of interest.

The DEM part is suggested to be used when the SM-level details are required, especially during fast transients when significant difference between SM voltages can be expected (when using permutation-based CBA for example). Also, the DEM should be used in the studies related to the CBA analysis.

Since it is practically impossible to initialize all the internal variables perfectly (for example, procedures in subsections III.A to III.F do not consider high-frequency effects), a short extraneous transient usually appears after model switching. To avoid possible negative effects of this on the simulation results, it is advised that a more detailed model that is used for the study be activated some moments before the disturbance representing a particular phenomenon in a network is applied. This allows the transient related to the activation of the model to die out and not affect the accuracy of the results. From the performed tests, 5 ms is usually enough for the transient to disappear.

2) Automated AVM Activation

The proposed AVM activation method uses grid frequency f_{PLL} (33) and DC voltage v_{DC} (34) error signals. When the deviations of the instantaneous signals from the respective moving average values are below a threshold ε_{MAX} (35) for a pre-specified period of time t_{tach} , it is considered that simulation is at quasi steady-state and therefore the AVM is activated to accelerate the simulation. More detailed models are activated manually in this paper. Error signals are defined as

$$\varepsilon_f = |f_{PLL} - f_0| / F_{nom} \quad (36)$$

$$\varepsilon_v = |v_{DC} - v_{DC0}| / V_{DCnom} \quad (37)$$

$$\varepsilon = \varepsilon_f + \varepsilon_v; \quad \varepsilon < \varepsilon_{MAX} \quad (38)$$

where ε_f and ε_v are the frequency and DC voltage errors; f_0

and v_{DC0} are moving average grid frequency and DC voltage values; F_{nom} and V_{DCnom} are nominal grid frequency and DC voltage, respectively; ε_{MAX} is maximal tolerable error.

The threshold value ε_{MAX} and the latch delay t_{latch} are chosen using a trial-and-error approach as the values that are small enough to detect transients in the DC voltage and AC frequency signals but large enough to allow for some slow variations in quasi-steady-state conditions.

In this paper, $\varepsilon_{MAX} = 0.001$, the moving average window duration for both f_0 and v_{DC0} is 0.1 s and $t_{latch} = 0.15$ s (latch delay in the AVM activation circuit, Fig. 8).

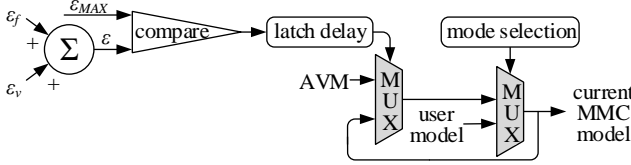


Fig. 8. Proposed automated AVM activation circuit.

IV. SIMULATION RESULTS

The proposed adaptive MMC model was implemented and tested in EMTP [23]. Simulations are performed on a point-to-point HVDC link shown in Fig. 9, system parameters are given in Table I, DC cable details are given in [5].

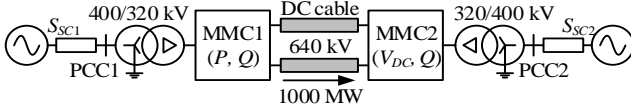


Fig. 9. Simulated point-to-point HVDC link.

TABLE I
SIMULATION PARAMETERS

Parameter	Nominal value	Symbol
Simulation time-step	5 μ s	Δt
Grid frequency (both grids)	$2\pi \times 50$ rad/s	ω
Grid voltage (both grids)	400 kV	V_{PCC}
Grid short-circuit level (both grids)	10 GVA	S_{SC}
DC voltage	640 kV	V_{DC}
Nominal converter power (both stations)	1000 MW	
Number of SMs per arm (HB / FB)	400 (80 / 320)	N_{SM}
Active power reference	1 pu	P_{ref}
Reactive power reference (both stations)	0 pu	Q_{ref}
DC voltage reference	1 pu	V_{DCref}
(ON / OFF)-resistance of IGBTs & diodes	1 m Ω / 1 M Ω	
Arm inductance	0.15 pu	L_{arm}
Transformer inductance	0.18 pu	L_{rfo}
Capacitor energy	40 kJ/MVA	
Permutations per time-step	1	N_0

A. Hybrid AEM and Pseudo-CBA Validation

To validate the developed Hybrid-AEM with Pseudo-CBA, the number of HB and FB SMs is set to 200 for demonstration purposes. AC voltage amplitude is set to be higher than DC voltage, so that FB SMs could be inserted negatively (Fig. 10).

When n_{ref} is negative (from t_1 to t_2), only FB SMs are inserted, so HB SM voltages remain constant. When the number of SMs to insert crosses zero and becomes positive again (at t_2), Pseudo-CBA keeps inserting only FB SMs

because their voltage is higher than HB voltage and arm current is discharging. When n_{ref} becomes greater than the number of FB SMs (at t_3), HB SM voltages start changing, indicating that HB SMs are also being inserted. AEM results closely match DEM results, which validates the proposed Hybrid-AEM.

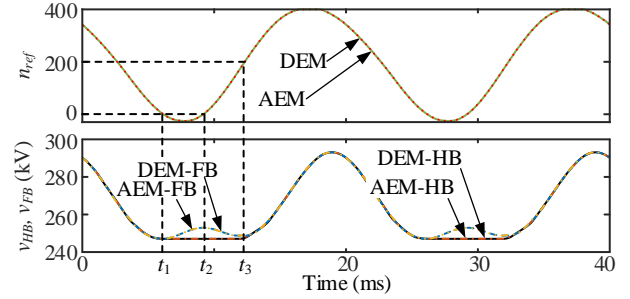


Fig. 10. Hybrid-AEM validation against the DEM (solid green: DEM, dotted red: AEM, dashed blue: AEM-FB, dash-double-dotted yellow: DEM-FB, dash-dotted orange: DEM-HB, solid black: AEM-HB).

B. Validation of DEM Memory Pointer Exchange

Two different CBAs are tested in Fig. 11: permutation-based CBA1 and voltage sorting-based CBA2. The address of G_j array provided by the CBA blocks is changed during runtime. Fig. 12 shows voltages of 10 SMs when switching from CBA1 to CBA2 at $t = 30$ ms. It takes CBA2 about 5 ms to considerably reduce differences in individual SM voltages. Therefore, memory pointer exchange approach is validated.

As it has been outlined in subsection III.C, the application of the voltage sorting-based CBA results in SM voltages being much closer to each other and therefore to the average value.

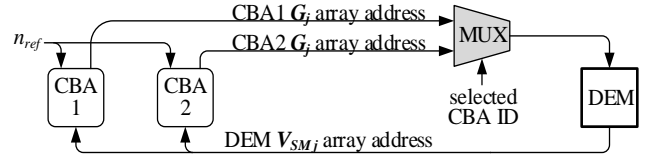


Fig. 11. Sample setup for switching between different CBA modules.

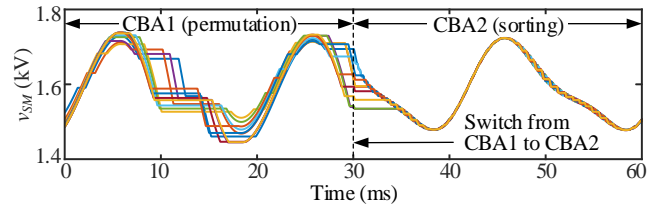


Fig. 12. SM voltages when switching between CBA modules.

C. Validation of arm AVMs

Both arm AVMs are validated against the DEM, the AEM results are also shown for comparison. At first, 50% active power step is applied to MMC1 in Fig. 13. Arm AVMs' results match with the DEM and AEM except for 100 Hz ripple in difference current $i_{diff a} = (i_{ua} + i_{va})/2$ associated with CCSC.

Next, a 150 ms 3-phase fault is applied at PCC2, results are shown in Fig. 14. Higher frequency transients in DC current and voltage are not well represented with arm AVMs, but results match in lower-frequency transients and at steady-state.

The relative errors of the arm AVMs and AEM compared to the DEM are shown in Table II. The AEM has a good

agreement with the DEM in all cases whereas the arm AVMs' results are close to the DEM during slow transients such as in Fig. 13 and deviate considerably during large transients, such as in Fig. 14. In all cases, the Arm-AVM-1 and Arm-AVM-2 results are very close to each other.

TABLE II
MAXIMAL RELATIVE ERROR OF THE CONSTITUTING MODELS (%)

Model	P_{PCC1}	$i_{diff a}$	i_{DC}	v_{DC}
AEM	0.02	0.42	1.63	0.32
Arm-AVM-1	1.09	5.80	42.8	2.70
Arm-AVM-2	1.09	5.83	42.6	2.62

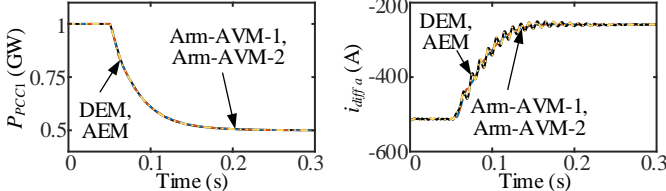


Fig. 13. Power step at MMC1 (dashed blue: Arm-AVM-1, dash-dotted orange: Arm-AVM-2, dash-double-dotted yellow: AEM, solid black: DEM).

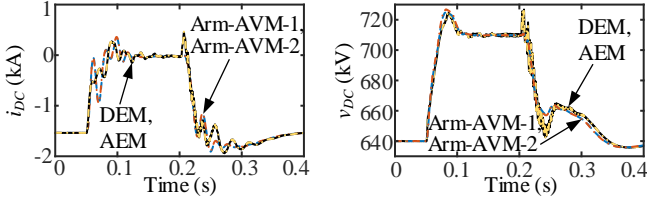


Fig. 14. AC fault at PCC2 (dashed blue: Arm-AVM-1, dash-dotted orange: Arm-AVM-2, dash-double-dotted yellow: AEM, solid black: DEM).

D. Computing Times

The HVDC link shown in Fig. 9 is simulated in normal operation mode for 1 s and computing times with different models are shown in Table III.

Models that do not represent SM-level details have constant computing times. Computing time of the DEM depends linearly on the number of SMs in case of permutation-based CBA and quadratically in case of voltage sorting-based CBA. Memory pointer exchange saves 15%–20% of simulation time with permutation CBA. Acceleration factor relatively to the DEM depends on N_{SM} and can reach 20 with voltage sorting CBA.

Acceleration factor can be further improved if a variable time-step simulation scheme is implemented for the AVM, since it can operate with Δt as large as 50 μ s or 100 μ s [5].

TABLE III
COMPUTING TIMES WITH DIFFERENT MMC MODELS (s)

N_{SM}	Arm-AVM-1	Arm-AVM-2	AEM	mem. pointer		default DEM	
				permutation	sorting	permutation	sorting
100	18.04	19.56	21.31	38.51	46.31	40.05	48.44
300	18.16	19.69	21.31	69.29	174.12	80.55	184.87
500	18.19	19.69	21.51	98.96	408.26	122.70	430.28

E. DC Fault

A DC fault is applied in the middle of the DC cable at 0.5 s and the results with the DM, DEM, and the proposed adaptive model are compared in Fig. 15 and Fig. 16. There is a close match between all models even at SM level. CPU time for 0.6 s of simulation with the adaptive model is 16.8 s, with the DEM it is 167 s, and with the DM it is 33739 s, yielding 9.9 acceleration factor if compared to the DEM-only model and 2008 relative to the DM.

The accuracy of the adaptive model is validated using the maximal relative difference compared to the reference models during the whole simulation except the initialization transient. The results are shown in Table IV (v_{Ctot} and i_{arm} of phase A upper arm at MMC1 are taken). The largest error is in the value of the arm current with the DM. This error is caused by a slight shift in time (10 μ s) between the peak values, which are practically identical: 2830 A for the adaptive model and 2847 A for the DM (difference is less than 1%).

TABLE IV
MAXIMAL RELATIVE ERROR OF THE ADAPTIVE MODEL (%)

Reference model	v_{DC}	v_{Ctot}	i_{arm}
DM	2.59	0.22	6.30
DEM-only	1.46	0.10	0.30

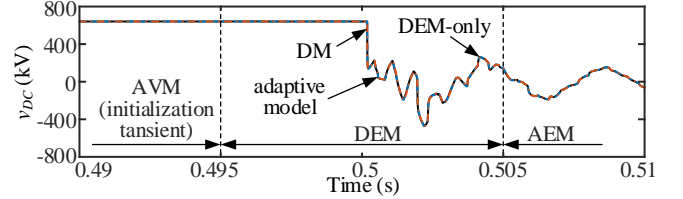


Fig. 15. MMC1 DC voltage during DC fault (dashed blue: proposed adaptive model, dash-dotted orange: DEM, solid black: DM).

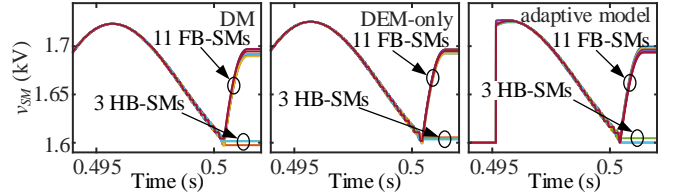


Fig. 16. Voltages of 14 SMs in phase A upper arm, MMC1. Sorting CBA.

F. Small-Scale AC Grid

The small-scale AC grid in Fig. 17, developed from the system presented in [24], includes synchronous generators with voltage regulators and governors, transmission lines, transformers, and impedance loads. A 3-phase fault occurs at 2 s when the system is at quasi-steady-state. The fault is cleared with 100 ms delay by tripping the line between ALIAG and SOMA buses. The simulation is performed with the proposed adaptive model, with the DEM, and with the DM. Permutation is applied once every four time-steps.

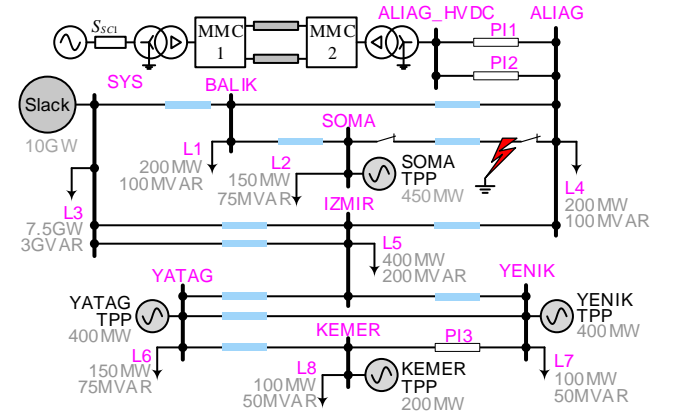


Fig. 17. Simulated small scale AC grid.

The switching instants of the proposed adaptive model are demonstrated in Fig. 18. The Arm-AEM-2 is used during the initialization transient. The DEM is manually activated at

$t_1 = 1.95$ s for 10 ms to study SM voltages in the first instants of the fault. The AEM is then manually activated at $t_2 = 2.05$ s and the automated AVM activation circuit is turned on. At $t_3 = 2.43$ s the error signal ε (35) falls below the maximal tolerable value ε_{MAX} and after t_{latch} (at $t_4 = 2.58$ s) the Arm-AVM-2 is automatically activated till the simulation ends.

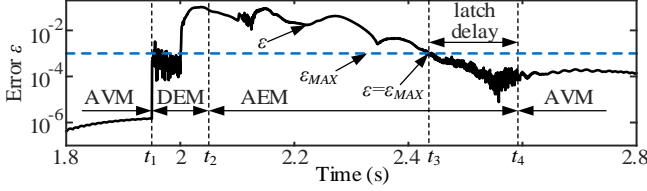


Fig. 18. Switching instants and models for MMC2.

The voltages of 14 uniformly selected SMs obtained with the adaptive model in Fig. 19 match the SM voltages obtained with the DEM and DM, and the maximum SM voltage has almost identical value. Fast transients in the DC current and voltage with the adaptive model are in good agreement when compared to DEM and DM in Fig. 20. Generator power obtained using the adaptive model also matches both references, Fig. 21.

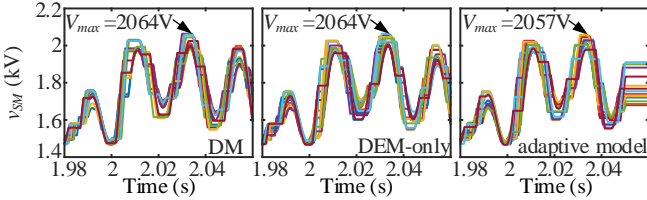


Fig. 19. Voltages of 14 SMs in phase B upper arm, MMC2. Permutation CBA.

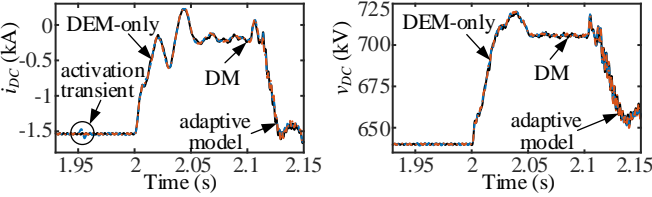


Fig. 20. MMC2 DC current and voltage during fast transient (dashed blue: proposed adaptive model, dash-dotted orange: DEM, solid black: DM).

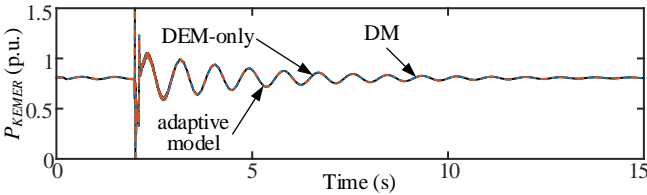


Fig. 21. Active power at KEMER TPP (dashed blue: proposed adaptive model, dash-dotted orange: DEM, solid black: DM).

The computing time of the performed study using the DM is 701021 s (8 days), using DEM only it is 1804 s, whereas the proposed model takes 509 s. This results in acceleration factors of 3.5 compared to the DEM and 1377 compared to the DM.

Error analysis is shown in Table V. As in the DC fault case, relatively large errors in power and current are caused by a slight shift in time (below 70 μ s) between waveforms. When accounted for the time-shift, the errors are below 1%.

TABLE V
MAXIMAL RELATIVE ERROR OF THE ADAPTIVE MODEL (%)

Reference model	i_{DC}	v_{DC}
DM	5.33	0.66
DEM-only	3.74	0.54

V. CONCLUSION

This paper presents an adaptive model of modular multilevel converters for electromagnetic transient simulations. It comprises two novel arm AVMs, Hybrid-AEM with Pseudo-CBA, and DEM with memory pointer exchange implementation. The adaptive model allows for seamless transitions between different levels of details and control systems during simulations. The adaptive model is applicable to half-bridge, full-bridge, and hybrid MMCs with arbitrary proportions of half-bridge SMs.

The highest accuracy is delivered by the DEM part of the adaptive model, which is activated when the highest level of details is necessary. Computational acceleration compared to the standalone DEM comes from the usage of simplified parts in the adaptive model during simulation intervals when SM-level details are not necessary, such as the slower electromechanical transients and the initialization transients.

Validation of the adaptive model and acceleration gains are provided using realistic test cases. The acceleration gains have reached values as high as 9.9 in the presented tests when compared to the DEM and above 2000 when compared to the DM, while keeping comparable level of accuracy.

VI. APPENDIX

To activate the AEM or DEM part of the adaptive model when passing from the AVM, the instantaneous values of the sum of all SM voltages per arm v_{Ctor} and of the arm switching function s are necessary. To find them, it is proposed to adapt the algorithm from [21], which is based on the arm current and voltage DC and fundamental components (I_0 , \bar{I}_1 , V_0 , \bar{V}_1).

The DC components for the algorithm are readily available in both arm AVMs ($I_0 = i_{arm}^{DC}$, $V_0 = v_{CAVM}$) and the fundamental frequency AC phasors $\bar{I}_1 = I_1 \angle \phi_I$ and $\bar{V}_1 = V_1 \angle \phi_V$ are estimated from two adjacent time-points x and y assuming balanced steady-state conditions. For the AC current phasor:

$$i_x = i_{arm}^{AC}(t - \Delta t) = I_1 \cos(\omega[t - \Delta t] + \phi) \quad (39)$$

$$i_y = i_{arm}^{AC}(t) = I_1 \cos(\omega t + \phi) \quad (40)$$

Applying trigonometric sum and product formulas to (39) and (40), the phasor amplitude and phase angle are obtained

$$I_1 = \sqrt{\left[i_x / \sin(\omega \Delta t) - i_y \cot(\omega \Delta t) \right]^2 + i_y^2} \quad (41)$$

$$\phi_I = \text{atan2}\left(i_x / \sin(\omega \Delta t) - i_y \cot(\omega \Delta t), i_y \right) \quad (42)$$

Formulas similar to (39)–(42) are used to obtain the AC voltage phasor \bar{V}_1 . To find the v_{Ctor} and s values, the following system of five complex nonlinear equations from [21] is solved:

$$\bar{V}_{Ctor1} = N_{SM} \left[\bar{I}_1 S_0 + I_0 \bar{S}_1 + \bar{I}_1^* \bar{S}_2 / 2 \right] / [j\omega C_{SM}] \quad (43)$$

$$\bar{V}_{Ctor2} = N_{SM} \left[I_0 \bar{S}_2 + \bar{I}_1 \bar{S}_1 / 2 \right] / [2j\omega C_{SM}] \quad (44)$$

$$\bar{S}_1 = \left[\bar{V}_1 - S_0 \bar{V}_{Ctor1} - \bar{S}_1^* \bar{V}_{Ctor2} / 2 - \bar{S}_2 \bar{V}_{Ctor1} / 2 \right] / V_{Ctor0} \quad (45)$$

$$V_{Ctot0} = \left[V_0 - \text{Re}(\bar{V}_{Ctot1} \bar{S}_1^* + \bar{V}_{Ctot2} \bar{S}_2^*) / 2 \right] / S_0 \quad (46)$$

$$\bar{S}_2 = - \left[S_0 \bar{V}_{Ctot2} + \bar{S}_1 \bar{V}_{Ctot1} / 2 \right] / V_{Ctot0} \quad (47)$$

where V_{Ctot0} , \bar{V}_{Ctot1} , and \bar{V}_{Ctot2} are the 0th, 1st, and 2nd harmonic phasors of the total capacitor voltage; S_0 , \bar{S}_1 , and \bar{S}_2 are the 0th, 1st, and 2nd harmonic phasors of the arm switching function; and the asterisk represents the complex conjugation.

It is proposed to solve (43)–(47) using a fixed-point iterative algorithm. More details on the implementation of this algorithm and on the derivation of (43)–(47) are given in [21]. The instantaneous values of v_{Ctot} and s are then found as

$$v_{Ctot} = V_{Ctot0} + \text{Re}(\bar{V}_{Ctot1}) + \text{Re}(\bar{V}_{Ctot2}) \quad (48)$$

$$s = S_0 + \text{Re}(\bar{S}_1) + \text{Re}(\bar{S}_2) \quad (49)$$

REFERENCES

- [1] A. Lesnicar and R. Marquardt, "An innovative modular multilevel converter topology suitable for a wide power range," in *2003 IEEE Bologna PowerTech - Conference Proceedings*, Bologna, Italy, 2003, pp. 272-277.
- [2] W. Lin, D. Jovicic, S. Nguefeu, and H. Saad, "Full-Bridge MMC Converter Optimal Design to HVDC Operational Requirements," *IEEE Transactions on Power Delivery*, vol. 31, pp. 1342-1350, Jun 2016.
- [3] S. Denetière, H. Saad, B. Clerc, and J. Mahseredjian, "Setup and performances of the real-time simulation platform connected to the INELFE control system," *Electric Power Systems Research*, vol. 138, pp. 180-187, Sep 2016.
- [4] Z. Li, F. Gao, F. Xu, X. Ma, Z. Chu, P. Wang, *et al.*, "Power module capacitor voltage balancing method for a±350-kV/1000-MW modular multilevel converter," *IEEE Transactions on Power Electronics*, vol. 31, pp. 3977-3984, 2016.
- [5] H. Saad, S. Denetière, J. Mahseredjian, P. Delarue, X. Guillaud, J. Peralta, *et al.*, "Modular Multilevel Converter Models for Electromagnetic Transients," *IEEE Trans. on Power Delivery*, vol. 29, pp. 1481-1489, June 2014.
- [6] B4.57, CIGRE Working Group, "Guide for the Development of Models for HVDC Converters in a HVDC Grid," vol. 1, ed. Paris, 2014, p. 221.
- [7] U. N. Gnanarathna, A. M. Gole, and R. P. Jayasinghe, "Efficient Modeling of Modular Multilevel HVDC Converters (MMC) on Electromagnetic Transient Simulation Programs," *IEEE Transactions on Power Delivery*, vol. 26, pp. 316-324, Jan 2011.
- [8] N. Ahmed, L. Angquist, S. Norrga, A. Antonopoulos, L. Harnefors, and H.-P. Nee, "A Computationally Efficient Continuous Model for the Modular Multilevel Converter," *IEEE Journal of Emerging and Selected Topics in Power Electronics*, vol. 2, pp. 1139-1148, Dec. 2014.
- [9] H. Saad, J. Peralta, S. Denetière, J. Mahseredjian, J. Jatskevich, J. A. Martinez, *et al.*, "Dynamic Averaged and Simplified Models for MMC-Based HVDC Transmission Systems," *IEEE Trans. on Power Delivery*, vol. 28, pp. 1723-1730, July 2013.
- [10] X. Jianzhong, Z. Chengyong, L. Wenjing, and G. Chunyi, "Accelerated model of modular multilevel converters in PSCAD/EMTDC," *IEEE Transactions on Power Delivery*, vol. 28, pp. 129-136, 2013.
- [11] S. P. Teeuwssen, "Simplified dynamic model of a voltage-sourced converter with modular multilevel converter design," in *2009 IEEE/PES Power Systems Conference and Exposition (PSCE 2009)*, Seattle, WA, USA, 2009, pp. 1-6.
- [12] F. B. Ajajei and R. Iravani, "Enhanced Equivalent Model of the Modular Multilevel Converter," *IEEE Transactions on Power Delivery*, vol. 30, pp. 666-673, 2015.
- [13] A. Beddard, C. Sheridan, M. Barnes, and T. Green, "Improved accuracy average value models of modular multilevel converters," *IEEE Transactions on Power Delivery*, vol. 31, pp. 2260-2269, 2016.
- [14] S. Yu, S. Zhang, Y. Wei, Y. Zhu, and Y. Sun, "Efficient and accurate hybrid model of modular multilevel converters for large MTDC systems," *IET Generation, Transmission & Distribution*, vol. 12, pp. 1565-1572, 2017.
- [15] X. Meng, J. Han, J. Pfannschmidt, L. Wang, W. Li, F. Zhang, *et al.*, "Combining Detailed Equivalent Model with Switching-Function-Based Average Value Model for Fast and Accurate Simulation of MMCs," *IEEE Transactions on Energy Conversion*, pp. 1-1, 2019.
- [16] S. Denetière, S. Nguefeu, H. Saad, and J. Mahseredjian, "Modeling of modular multilevel converters for the France-Spain link," presented at the IPST 2013, Vancouver, BC, Canada, 2013.
- [17] S. Rohner, S. Bernet, M. Hiller, and R. Sommer, "Modulation, losses, and semiconductor requirements of modular multilevel converters," *IEEE Transactions on Industrial Electronics*, vol. 57, pp. 2633-2642, 2010.
- [18] X. Shi, Z. Wang, B. Liu, Y. Li, L. M. Tolbert, and F. Wang, "Steady-State Modeling of Modular Multilevel Converter under Unbalanced Grid Conditions," *IEEE Transactions on Power Electronics*, vol. 32, pp. 7306-7324, 2017.
- [19] J. Wang, J. Liang, F. Gao, X. Dong, C. Wang, and B. Zhao, "A Closed-Loop Time-Domain Analysis Method for Modular Multilevel Converter," *IEEE Transactions on Power Electronics*, vol. 32, pp. 7494-7508, 2017.
- [20] A. Stepanov, H. Saad, U. Karaagac, and J. Mahseredjian, "Spurious Power Losses in Modular Multilevel Converter Arm Equivalent Model," *IEEE Transactions on Power Delivery*, pp. 1-9, 2019.
- [21] A. Stepanov, H. Saad, U. Karaagac, and J. Mahseredjian, "Initialization of Modular Multilevel Converter Models for the Simulation of Electromagnetic Transients," *IEEE Transactions on Power Delivery*, vol. 34, pp. 290-300, 2018.
- [22] A. Stepanov, H. Saad, J. Mahseredjian, and A. Wataré, "Overview of Generic HVDC-MMC Control under Unbalanced Grid Conditions," presented at the International Power Systems Transients Conference (IPST 2017), Seoul, South Korea, 2017.
- [23] J. Mahseredjian, S. Denetière, L. Dubé, B. Khodabakhchian, and L. Gérin-Lajoie, "On a new approach for the simulation of transients in power systems," *Electric Power Systems Research*, vol. 77, pp. 1514-1520, Sep. 2007.
- [24] U. Karaagac, J. Mahseredjian, and O. Saad, "An Efficient Synchronous Machine Model for Electromagnetic Transients," *IEEE Transactions on Power Delivery*, vol. 26, pp. 2456-2465, 2011.